THE JOURNAL OF PHYSICAL CHEMISTRY A

Article

pubs.acs.org/JPCA

Three-Dimensional Ab Initio Potential Energy Surface for H−CO($\tilde{X}^2A'$)

Lei Song, Ad van der Avoird, and Gerrit C. Groenenboom*

Theoretical Chemistry, Institute for Molecules and Materials, Radboud University Nijmegen, Heyendaalseweg 135, 6525 AJ Nijmegen, The Netherlands

Supporting Information

ABSTRACT: We present an ab initio potential for the H−CO($\tilde{X}^2A'$) complex in which the CO bond length is varied and the long-range interactions between H and CO are accurately represented. It was computed using the spin-unrestricted open-shell single and double excitation coupled cluster method with perturbative triples [RHF-UCCSD(T)]. Three doubly augmented correlation-consistent basis sets were utilized to extrapolate the correlation energy to the complete basis set limit. More than 4400 data points were calculated and used for an analytic fit of the potential: long-range terms with inverse power dependence on the H−CO distance R were fit to the data points for large R, the reproducing kernel Hilbert space (RKHS) method was applied to the data at smaller distances. Our potential was compared with previous calculations and with some data extracted from spectroscopy. Furthermore, it was used in three-dimensional discrete variable representation (DVR) calculations of the vibrational frequencies and rotational constants of HCO, which agree very well with the most recently measured data. Also the dissociation energy D_0 = 0.623 eV of HCO into H + CO obtained from these calculations agrees well with experimental values. Finally, we made preliminary two-dimensional (2D) calculations of the cross sections for rotationally inelastic H−CO collisions with the CO bond length fixed and obtained good agreement with recently published 2D results.

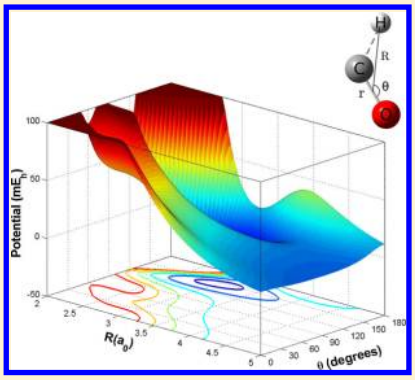

1. INTRODUCTION

As the second most abundant molecule in the universe, carbon monoxide (CO) is typically observed in star-forming regions and protoplanetary disks, and in external galaxies. It is commonly used as a tracer of physical conditions in the regions where CO infrared emission is observed. To extract astrophysical parameters from the observed spectral lines, it is often not appropriate to assume local thermodynamic equilibrium (LTE) in the dilute gas of astronomical sources. Non-LTE methods used to analyze the available observations require collisional rate coefficients.[1,2] The interpretation of the observed CO spectral lines critically relies on the collisional rate coefficients of CO with the dominant collision partners: H, H_2, and He.[3,4] These rate coefficients can be obtained from scattering calculations based on potentials of CO with its collision partners, thus accurate potential energy surfaces (PESs) are urgently needed.

Compared with CO−H_2 or CO−He, the interaction between CO and H is relatively strong and the equilibrium CO bond length in HCO is substantially larger than in free CO. Hence, a three-dimensional (3D) potential with CO bond length dependence is needed. Pioneering work on the dynamics of HCO based on the 3D BBH potential constructed by Bowman, Bitman, and Harding was carried out by Bowman and co-workers.[5−7] Werner et al. discovered later that the BBH potential and its empirically modified versions[6,7] did not reproduce well the spectroscopic data of Tobiason et al.,[8] so they developed the 3D Werner-Keller-Schinke (WKS) potential.[9,10] This potential was based on elaborate high-quality complete active space self-consistent field (CASSCF) and multireference configuration interaction (MRCI) calculations, with special attention for the conical intersections between the potentials of different electronic states. Much theoretical[5−7,9−13] and experimental[8,14−19] work has been devoted to the study of resonances that play an important role in the photodissociation of HCO into H + CO. Classical and (approximate) quantum mechanical scattering calculations[20−22] studying the rotational and vibrational (de)excitation of CO in collisions with hot H atoms have been performed with both the BBH and WKS potentials. It was found that the well region of the potential is important especially for vibrationally inelastic collisions, and that the rotationally inelastic scattering cross sections deviated from experimental data probably because the van der Waals region of the potential was insufficiently accurate.

In the present paper we focus on the lower energy region of the HCO potential surface. The cross sections for rotational and vibrational (de)excitation of CO in collisions with H atoms are important for astrophysical modeling. Shepler et al.[23] have shown recently that the rotationally inelastic H−CO collision cross sections critically depend on the long-range behavior of the PES, especially for collisions at low energies. Calculations

Special Issue: Joel M. Bowman Festschrift

Received: March 11, 2013
Revised: April 17, 2013
Published: April 18, 2013

on the WKS potential produced much larger values of these cross sections than on the BBH potential and also disagree with the cross sections computed by Shepler et al. on their CCSD(T) and MRCI potentials. The analysis in ref 23 shows that the reason for this discrepancy is that the WKS potential does not reflect well the anisotropic long-range van der Waals interaction. Shepler et al. paid much attention to make their potentials describe the correct long-range behavior, but they only produced two-dimensional (2D) potentials[23] with the CO bond length fixed.

The goal of this Article is to provide an accurate 3D ab initio potential energy surface of the H−CO complex in the ground state ($\tilde{X}^2A'$) with explicit consideration of the long-range behavior. Details of the ab initio electronic structure calculations are given in the next section. Section 3 describes the fit procedure and shows the accuracy of the fit. In Section 4.1, we present our potential, compare it with previous studies, and discuss some properties. Furthermore, we compare in this section the rotationally inelastic H−CO collision cross sections computed on our potential with results obtained on the 2D potentials of Shepler et al. In Section 4.2 we use our potential surface to compute the vibrational frequencies and rotational constants of HCO by means of a 3D discrete variable representation (DVR) method, and we show that they are in good agreement with the best available experimental data. The conclusion and outlook are given in Section 5.

2. AB INITIO CALCULATIONS

In order to explore the structure of the global potential energy surface, we first performed state-averaged CASSCF[24,25] calculations. The goal of these calculations was to identify conical intersections of the ground state potential of A' symmetry with the potentials that correlate with the lowest excited Π state of CO. Starting with orbitals from restricted Hartree−Fock (RHF) calculations in an augmented correlation-consistent polarized valence quadruple-ζ (aug-cc-pVQZ) basis[26] we performed three-state averaged full valence CASSCF calculations with 11 electrons in 9 active orbitals. They revealed the existence of a conical intersection at nonlinearity, in addition to those that were already found at the linear H−CO and CO−H structures.[9,10] However, all of these intersections occur at considerably higher energies than the lowest conical intersection identified by Werner et al., which occurs at approximately 1.4 eV ≈ 11000 cm^{-1} above the H + CO asymptotic limit.[9,10] Since we are interested in H−CO collisions for rotational and $v = 0 \rightarrow 1$ vibrational (de)-excitation of CO at lower collision energies, we may assume that we only need the ground-state potential of A' symmetry in the energy region well below all conical intersections. Full CASSCF and MRCI calculations as performed by Werner et al.[9,10] are therefore not needed. On the other hand, we wish our potential to be especially accurate in the long-range, so we had to use a method that is size-extensive (see ref 27, Section 13.3). We adopted the spin-unrestricted open-shell single and double excitation coupled cluster method[28,29] with perturbative triples[30] [UCCSD(T)], with the molecular orbitals from RHF calculations. Some further discussion on the effects of the conical intersections is given below, after the presentation of our calculated potential and its analytic fit.

The ab initio electronic structure calculations were performed with the MOLPRO 2000 package.[31] Doubly augmented correlation-consistent d-aug-cc-pVnZ basis sets[26] were used with $n = 3$, 4, and 5, and the correlation energy was extrapolated to the complete basis set (CBS) limit.[32,33] The H−CO interaction energy was calculated with the Boys and Bernardi counterpoise correction to avoid the basis-set superposition error[34] (BSSE), i.e., the interaction energies were determined as $E_{HCO}-E_{CO}-E_H$, with the H and CO monomers computed in the same one-electron basis as the H−CO dimer. In total, we calculated 4428 interaction energies: 3744 grid points used in the fit and 684 random points to test the fit.

The grid is based on three Jacobi coordinates, shown in Figure 1: the CO bond length r, the distance R, i.e., the length

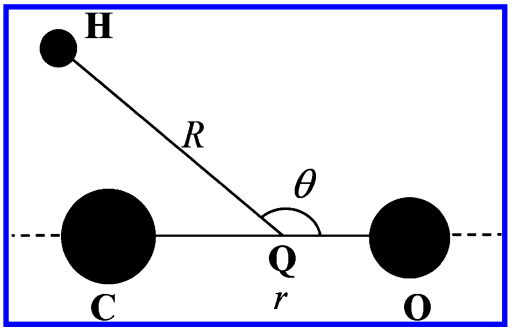

Figure 1. Jacobi coordinates for H−CO; Q denotes the CO center of mass.

of the vector **R** pointing from the center of mass of CO to the H nucleus, and the angle θ between **R** and the CO axis **r**. For θ we employed 13 Gauss-Legendre quadrature points in the range from 0° to 180°. We chose 32 points for the R coordinate from 2.0 a_0 to 20.0 a_0. In the range of 2.0 $a_0 \le R < 6.0$ a_0, the step size ΔR is 0.2 a_0, while ΔR equals 0.4 a_0 in the range of 6.0 $a_0 \le R < 8.0$ a_0. A logarithmically spaced grid with seven points is applied for the range of 8.0 $a_0 \le R \le 20.0$ a_0. The vibrational coordinate r is varied from 1.65 a_0 to 2.85 a_0, including 1.65, 1.85, 2.05, 2.1322, 2.20, 2.25, 2.45, 2.65, and 2.85 a_0.

We note that the RHF-UCCSD(T) method is a single-reference electron correlation method, which will fail near the conical intersections and in the CO bond dissociation region. The so-called T_1 diagnostic[35−37] is a measure for the amount of multireference behavior; the larger the value of this T_1 diagnostic, the less reliable the results from the single-reference electron correlation method are. In this work, we removed or reduced the weight of five ab initio points, because of their bad T_1 diagnostic (ranging from 0.085 to 0.142).

3. FIT PROCEDURE

The 3D H−CO potential is written as the sum of the CO diatomic potential and the interaction energy between H and CO

$$V_{HCO}(r, R, \theta) = V_{CO}(r) + V_{int}(r, R, \theta) \quad (1)$$

The CO diatomic molecule potential $V_{CO}(r)$ was obtained from the vibrational energies G_v and rotational constants B_v measured by Le Floch[38] by means of the first-order semiclassical Rydberg−Klein−Rees (RKR) procedure, as implemented by Le Roy.[39] The analytical H−CO interaction potential $V_{int}(r,R,\theta)$ was obtained from a fit to our ab initio RHF-UCCSD(T) H−CO interaction energies. We first fitted its θ-dependence, then its R-dependence, and finally its r-dependence, with the following procedure.

dx.doi.org/10.1021/jp402470b | J. Phys. Chem. A 2013, 117, 7571−7579

Table 1. Coefficients $V_{nl}^{(lr)}(r)$ [in $E_h a_0^n$] of the Long-Range R^{-n} Terms in Eq 4 Obtained from Our Fits (See Section 3) with l Denoting the Indices of the Legendre Polynomials $P_l(\cos\theta)$ That Represent the Angular Dependence of the Potential

r	$V_{6,0}$	$V_{6,2}$	$V_{7,1}$	$V_{7,3}$	$V_{8,4}$	$V_{9,5}$
1.65	18.62154	0.62830	−81.20027	−1.27329	4.35816	−61.11080
1.85	19.58438	0.75523	−75.33132	0.69718	0.31787	2.50351
2.05	20.90374	1.06060	−70.39766	2.72797	3.89982	290.03122
2.1322	21.22015	1.42621	−70.30271	4.75132	−22.07285	230.87453
2.20	21.83178	1.69050	−60.18380	3.94278	−45.09345	−1267.90953
2.25	22.09369	1.63455	−65.00574	4.60370	−20.28939	188.78523
2.45	23.80770	2.58206	−63.52498	4.47302	3.20559	247.74622
2.65	25.32512	3.50240	−64.28439	2.06188	−0.55607	−44.36051
2.85	25.56625	4.61577	−68.00236	0.90311	−9.14573	−85.05427

The θ-dependence of the interaction energy for each of the (r,R) points was expanded as

$$V_{\text{int}}(r, R, \theta) = \sum_{l=0}^{12} V_l(r, R) P_l(\cos\theta) \tag{2}$$

where the $P_l(\cos\theta)$ are Legendre polynomials with $l = 0-12$. The expansion coefficients $V_l(r,R)$ are calculated by means of a 13-point Gauss-Legendre quadrature when the vibrational coordinate r is $\leq 2.20\ a_0$. For larger r, five points with T_1 diagnostic larger than 0.085 were removed or weighted by a factor less than 0.01 in the fit process. In this case, the Gauss-Legendre quadrature grid is incomplete, so another method is needed. We employed the linear least-squares fitting procedure with Tikhonov regularization[40] in which the term $\alpha\Sigma_l l^2 V_l(r,R)|^2$ is added to the residual. The factor α was set to 10^{-10} to ensure that strong oscillations (associated with large l values) are damped out in the fit.

Then, we represented the coefficients $V_l(r,R)$ by analytical functions of R, for each value of r. For the terms with $l \leq 5$, the long-range and short-range contributions were fit separately, and summed

$$V_l(r, R) = V_l^{(lr)}(r, R) + V_l^{(sr)}(r, R) \tag{3}$$

The dominant long-range interactions between H and CO are dispersion forces. Smaller contributions are the interactions between the (small) dipole and higher multipoles of CO and the multipole moments induced on the H atom. From perturbation theory with the interaction operator in the multipole expansion, it follows that all of these long-range interactions depend on the H−CO distance as R^{-n}, with the leading term having $n = 6$. The theory shows, moreover,[41] that this leading power n depends on the anisotropy of the interaction, as defined by the index l in the angular expansion of eq 2. We took this relation into account in our fit of the analytic form

$$V_l^{(lr)}(r, R) = \sum_n -V_{nl}^{(lr)}(r) f_n(\beta R) R^{-n} \tag{4}$$

to the long-range data for $R > 10\ a_0$. Only terms with even $n + l$ were included. For $l = 0$, 2 the inverse powers n of R^{-n} start with $n_i = 6$, while for $l = 1$, 3 the first term has $n_i = 7$. When $l \geq 4$, n begins with $n_i = l + 4$. Only the leading term with R^{-n_i} was included in $V_l^{(lr)}(R,r)$; the coefficient $V_{n_i l}^{(lr)}(r)$ of this term was obtained from a least-squares fit of the first two terms with R^{-n_i} and R^{-n_i-2} in eq 4 to the energies at the five long-range R values with $R > 10\ a_0$. The coefficient of the second term changed considerably when this fit was restricted to a subset of these long-range R values, while that of the leading term remained practically the same. Therefore, we included only the latter. The long-range coefficients $V_{nl}^{(lr)}(r)$ obtained from our fits for all values of r are listed in Table 1. The functions $f_n(\beta R)$ are Tang−Toennies damping functions[42] defined as

$$f_n(x) = 1 - e^{-x} \sum_{k=0}^{n} \frac{x^k}{k!} \tag{5}$$

with $x = \beta R$ and the parameter β set to $2.0 a_0^{-1}$. They suppress the singular behavior of the long-range terms in the short-range. No explicit long-range contributions were calculated for $l > 5$.

After subtraction of the long-range contributions with $l \leq 5$ from $V_l(r,R)$, the short-range contributions $V_l^{(sr)}(r,R)$ were obtained for each value of r by interpolation over the full range of R with the reproducing kernel Hilbert space (RKHS) method.[43,44] The smoothness parameter n of the RKHS method (see eq 9 in ref 43) was fixed to 2, while the RKHS parameter m that determines the asymptotic behavior of $V_l^{(sr)}(r,R)$ was chosen to depend on the value of l. For $l \leq 5$, m was set to n_i+1, so $V_l^{(sr)}(r,R)$ decays asymptotically as R^{-n_i-2}. For $l > 5$, where no separate long-range contributions were calculated, m was set to n_i-1, so that $V_l(r,R)$ decays as R^{-n_i}.

Finally, the values of the potential $V_{\text{int}}(r_p,R_i,\theta_j)$ on the grid points r_p, calculated at arbitrary values of R_i,θ_j with the functions obtained from the previous fits in θ and R, were fitted to a polynomial expansion

$$V_{\text{int}}(r, R_i, \theta_j) = \sum_{k=0}^{5} C_k(R_i, \theta_j) P_k(Ar + B) \tag{6}$$

The orthogonal polynomials $P_k(Ar+B)$ are Legendre polynomials in the coordinate $Ar + B$ with scaling parameters A and B chosen such that the range $1.65\ a_0 \leq r \leq 2.85\ a_0$ is linearly mapped onto the required interval from -1 to $+1$. The expansion coefficients $C_k(R_i,\theta_j)$ were obtained from a weighted linear least-squares fit. Points with higher energies ($V_{\text{int}} > 0.1\ E_h$) are less important in bound state and lower energy scattering calculations, so we chose an exponentially decreasing weight

$$w = e^{-\gamma(V_{\text{int}}-0.1)} \tag{7}$$

for those points, with $\gamma = 4$ and all quantities in the exponent given in E_h. The fit accuracy and the correct short-range repulsive behavior are conserved by this procedure.

The accuracy of the fit was tested in two ways. First, by comparison of potential energies from the fit with the ab initio values used, for all data points with $V_{\text{int}}(r_p,R_i,\theta_j) \leq 0.1\ E_h$, but with the exclusion of the five points that had bad T_1 diagnostics. The root-mean-square error (RMSE) defined by

dx.doi.org/10.1021/jp402470b | J. Phys. Chem. A 2013, 117, 7571−7579

$$\mathrm{RMSE} = \sqrt{\frac{1}{n}\sum_{p,i,j} |V_{\mathrm{int}}^{\mathrm{fit}}(r_p, R_i, \theta_j) - V_{\mathrm{int}}^{\mathrm{ab\ initio}}(r_p, R_i, \theta_j)|^2} \quad (8)$$

is 1.31×10^{-4} E_h for 2944 points in the short and middle range ($2.0\ a_0 \leq R \leq 10.0\ a_0$). The RMSE relative to the mean absolute values of V_{int} for each value of R in this range is 0.29%. For the long range ($R > 10.0\ a_0$), the absolute RMSE is 2.66×10^{-9} E_h for 585 points, and the relative RMSE is 0.20%. Second, we calculated 684 additional random points to test the fit. With the exclusion of the points with energy $V_{\mathrm{int}} > 0.1$ E_h or bad T_1 diagnostics (>0.085), 662 random points were used in this analysis. The RMSE is 3.25×10^{-4} E_h over 294 points in the short and middle range, and 2.61×10^{-8} E_h over 368 points in the long-range; the overall relative RMSE is 0.56%.

The Fortran code to evaluate our 3D H−CO intermolecular potential $V_{\mathrm{int}}(r,R,\theta)$ and the accurate RKR potential $V_{\mathrm{CO}}(r)$ is made available as Supporting Information.

4. RESULTS AND DISCUSSION

In order to check first for how large an r value we can still trust the RHF-UCCSD(T)/CBS method used to compute our 3D H−CO potential and how accurate the RHF-UCCSD(T) potential is, we computed the vibrational levels and wave functions of the free CO molecule on the empirical RKR potential and on a potential computed for free CO by the same RHF-UCCSD(T)/CBS method as used in the calculations on H−CO. Figure 2 shows the two potentials; for all r up to 3.05 a_0 they agree very well with each other. The calculations of the vibrational states were performed with the sinc-function discrete variable representation (sinc-DVR) method.[45,46] The vibrational wave function of CO with $v = 15$ is shown in Figure 2. With the vibrational wave functions obtained, we also calculated the rotational constants B_v of the different vibrational states v, and we compared the vibrational transition frequencies $G_v - G_{v-1}$ and rotational constants B_v with the experimental data.[47,48] For $v \leq 15$, the relative errors in $G_v - G_{v-1}$ from the empirical RKR potential derived from these frequencies are less than 0.001%; the errors in the *ab initio* results based on the RHF-UCCSD(T) potential are less than 0.3%. The relative errors in B_v with respect to the experimental values[38,49] are less than 0.02% for the RKR potential and less than 0.5% for the RHF-UCCSD(T) potential. This assessment shows that the RHF-UCCSD(T)/CBS method yields accurate potentials and that it is still reliable up to $r = 3.05\ a_0$. Furthermore, it confirms the accuracy of the semiclassical RKR potential, which is used as a building block in our 3D H−CO potential.

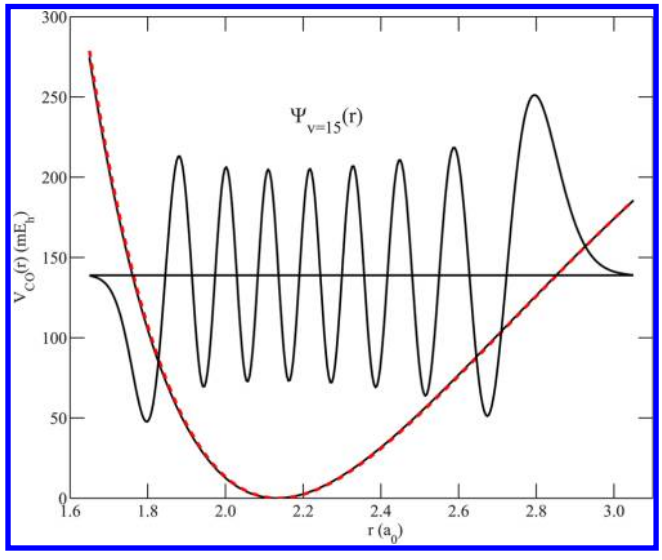

Figure 2. Empirical RKR potential $V_{\mathrm{CO}}(r)$ (solid line) and calculated RHF-UCCSD(T) potential (dashed line), with the $v = 15$ vibrational wave function calculated on the RKR potential.

4.1. Potential Surface. Figure 3 shows a 2D contour map of the H−CO potential in milli-hartree (mE_h) with r fixed at the experimental equilibrium bond length[38] $r_e = 2.1322\ a_0$ of the free CO molecule. The minimum (with depth −26.58 mE_h) marked with the black cross occurs at $R = 3.007\ a_0$ and $\theta = 144.8°$. The corresponding properties of the full 3D potential V_{HCO} are given in Table 2. The global minimum in the 3D potential has a depth of −30.70 mE_h and corresponds to a stable HCO structure with $R_{\mathrm{CH}} = 2.115\ a_0$, $r = 2.221\ a_0$ and ∠HCO = 124.6° in valence coordinates. The corresponding Jacobi coordinates are $R = 3.021\ a_0$ and $\theta = 144.8°$. This minimum is deeper by 4.12 mE_h than the minimum in the 2D potential with r fixed at r_e, and the CO bond is substantially stretched. Table 2 shows that there is also shallow local minimum corresponding to a metastable HOC structure with energy +37.0 mE_h. Table 3 lists the geometry and height of the barrier to linearity (with $\theta = 180°$). We find a barrier of 7.961 mE_h located at $r = 2.232\ a_0$ and $R_{\mathrm{CH}} = 2.019\ a_0$ in valence coordinates, which corresponds to $R = 3.294\ a_0$ in Jacobi coordinates. Our results are in good agreement with previous theoretical values of Werner et al. and Keller et al.[9,10] and with the values of Austin et al. and Johns et al.[50,51] extracted from experimental data (see Tables 2 and 3). It should be kept in mind that the structure extracted from microwave spectra corresponds to a vibrationally averaged geometry, while the theoretical data in these tables refer to the equilibrium geometry. A more direct comparison with experimental data is made when we discuss the rotational constants obtained from 3D DVR calculations in Section 4.2. Our global HCO minimum is slightly deeper than the minimum in the WKS potential and about equally deep as that in the modified WKS potential obtained by adjusting the WKS potential to some experimental data. Also the local minimum at the metastable HOC structure agrees well with that in the modified WKS potential. Our barrier to linearity is somewhat lower than the barriers in both these potentials. Table 4 gives the location and height of the dissociation barrier of HCO into H + CO or, equivalently, of the activation barrier of the association reaction. This barrier occurs in our RHF-UCCSD(T) potential at nearly the same geometry as in the WKS and modified WKS potentials based on multiconfigurational CASSCF and MRCI calculations. Our dissociation barrier is lower than in the WKS potential and slightly higher than in the semiempirically modified WKS potential. The experimental activation energy[52] is lower than all of these theoretical values, but it was already pointed out in ref 10 that the uncertainty in the measured value is quite large. To illustrate some of the characteristics of our potential more clearly, we display in Figure 4 two other cuts of the 3D potential, with θ fixed at 144.8° (upper panel) and 180° (lower panel). These cuts show the global minimum and the saddle point at linearity.

At this point let us return to our discussion of the conical intersections in the first paragraph of Section 2. Our RHF-UCCSD(T) single-reference method cannot reproduce conical intersections, where the potentials of multiple electronic states

dx.doi.org/10.1021/jp402470b | J. Phys. Chem. A 2013, 117, 7571−7579

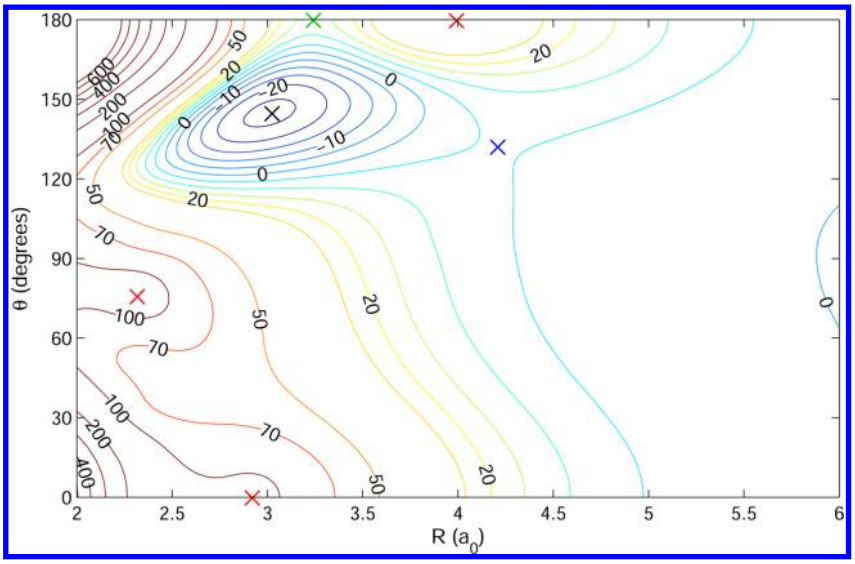

Figure 3. Contour plot of the V_{HCO} potential (in mE_h) with r fixed at the (experimental) equilibrium bond length r_e = 2.1322 a_0 of free CO. Energy zero is the energy of CO with bond length r_e and the H atom at infinite distance R. The black cross marks the minimum of depth −26.58 mE_h at R = 3.007 a_0 and θ = 144.8°, the green cross the barrier to linearity, and the blue cross the barrier to dissociation of H−CO. The red crosses show the locations of the local maxima related to the conical intersections between the ground electronic state and the first excited state.

Table 2. Comparison of the Global HCO and Local HOC Minima in Our Potential, in the WKS Potential,[9] and in the Modified WKS Potential,[10] and Experimental Values from Microwave Spectroscopy,[50] in Valence Coordinates

	WKS	modified WKS	our work	exp.
Global HCO Minimum				
R_{CH} [a_0]	2.112	2.110	2.115	2.098
r [a_0]	2.234	2.233	2.221	2.213
∠HCO [deg]	124.5	124.5	124.6	127.4
V_{HCO} [mE_h]	−28.9	−30.65	−30.70	−30.92 ± 0.3[a]
Local HOC Minimum				
R_{OH} [a_0]			1.845	
r [a_0]			2.427	
∠HOC [deg]			107.5	
V_{HCO} [mE_h]		38.1	37.0	

[a]Obtained from the experimental value of D_0[9,15] and the zero-point vibrational energies of HCO and CO from our calculations.

Table 3. Comparison of the Barrier to Linearity (∠HCO = 180°) in Our Potential, in the WKS Potential,[9] and in the Modified WKS Potential,[10] and Experimental Values from Electronic Absorption Spectroscopy,[51] in Valence Coordinates

	WKS	modified WKS	our work	exp.[a]
R_{CH} [a_0]	2.003	2.007	2.019	2.013
r [a_0]	2.250	2.248	2.232	2.234
V_{HCO} [mE_h]	12.0	9.853	7.961	

[a]The linear saddle point of the $\tilde{X}^2A'$ state is equivalent to the minimum of the $\tilde{A}^2A''$ state at linearity.

become degenerate, but we find a local maximum in our A' potential close to the location of the lowest conical intersection in the WKS potential of Werner et al.[9] The height of this maximum is not much lower than the energy of the conical intersection in the WKS potential. Also at the locations of the other conical intersections found in our CASSCF calculations, we find local maxima in our potential fitted to the RHF-UCCSD(T) calculations (see Figure 3). Furthermore, it was found in ref 9 that for linear geometries with shorter C−H bond lengths (and C−O bond lengths larger than the free CO equilibrium distance), the energy of the $^2\Pi$ state is lower than that of the $^2\Sigma$ state, so that the ground state A' potential becomes degenerate with the lowest A'' potential. The A'' state goes up in energy when the system becomes nonlinear, and the A' state goes down, so the lowest energy where these states are degenerate defines the barrier to linearity on the A' potential. Table 3 shows that the location of this barrier in our potential based on RHF-UCCSD(T) calculations is similar to the location of the barrier in the WKS potential based on CASSCF and MRCI calculations. The barrier (0.217 eV = 1747 cm^{-1} above the H + CO limit) in our potential is 34% lower than the barrier in the WKS potential, but only 19% lower than the barrier in the semiempirically adjusted WKS potential. When the energy of the system gets close to the height of this barrier one must, in principle, include the effects of Renner−Teller nonadiabatic coupling between the two degenerate electronic states.

Table 4. Comparison of the Barrier for HCO → H + CO Dissociation in Our Potential, in the WKS Potential,[9] and in the Modified WKS Potential,[10] in Valence Coordinates, as Well as the Experimental Activation Energy[52]

	WKS	modified WKS	our work	exp.
R_{CH} [a_0]	3.503	3.534	3.525	
r [a_0]	2.148	2.148	2.141	
∠HCO [deg]	117.1	117.0	116.0	
V_{HCO} [mE_h][a]	6.214	4.608	5.185	3.2 ± 0.6

[a]With respect to H and CO at infinite distance and CO at its equilibrium bond length.

In order to test our potential in the long range, we calculated integral cross sections for rotationally inelastic collisions of ground state CO(j = 0) with H atoms into the final states of CO with j' = 1, 2, ..., 11. We applied the quantum close-coupling method for collision energies of 400 and 800 cm^{-1}, and, in order to compare the results on our potential with cross

dx.doi.org/10.1021/jp402470b | J. Phys. Chem. A 2013, 117, 7571−7579

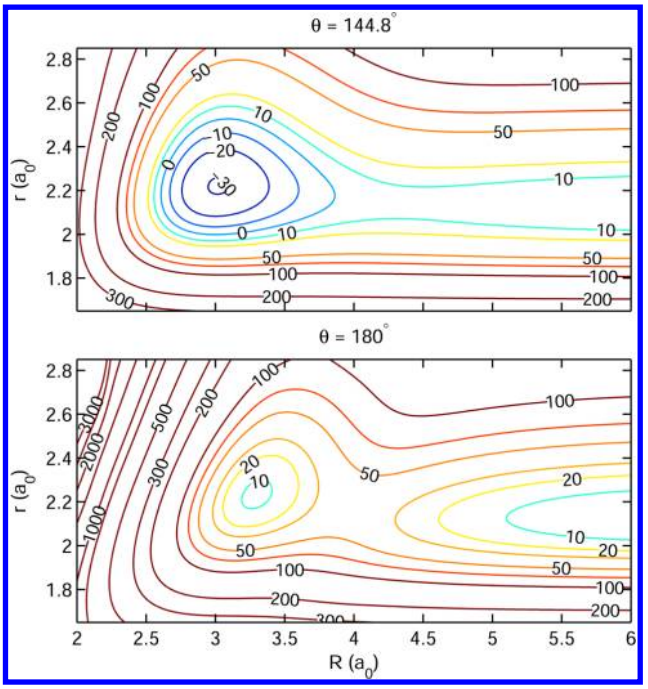

Figure 4. Contour plots of the V_{HCO} potential (in mE_h) with θ fixed at the equilibrium value of 144.8° (upper panel) and at 180° (linear geometry, lower panel).

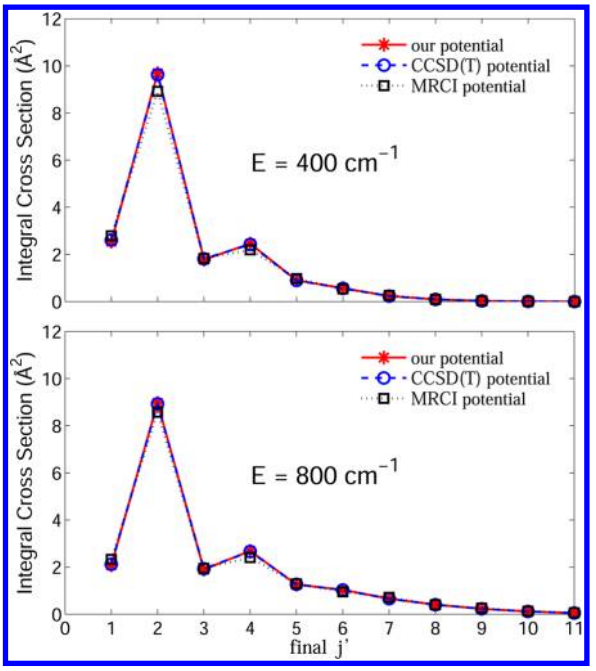

Figure 5. Integral cross sections for inelastic H−CO(v = 0, j = 0 → v = 0, j') scattering at collision energies of 400 cm^{-1} (upper panel) and 800 cm^{-1} (lower panel), obtained from close-coupling calculations in the rigid rotor approximation. For comparison with cross sections calculated on the 2D potentials of Shepler et al.[23] the CO bond length r was fixed at 2.1322 a_0 in our and in the CCSD(T) potential, while in the MRCI potential r was fixed at 2.20 a_0.

sections calculated on the 2D H−CO potentials of Shepler et al.,[23] CO was considered as a rigid rotor with r = 2.1322 a_0 (or 2.20 a_0 for the MRCI potential). The close-coupling equations were solved with the renormalized Numerov propagator with R ranging from 2.4 to 20 a_0 in steps of 0.02 a_0. The calculations were repeated with the R grid extended to 30 a_0 and steps of 0.05 a_0, but the results were practically the same. The channel basis included rotor functions of CO up to j = 20, and the calculations were made for overall angular momenta J = 0−60. Figure 5 shows for H−CO(j = 0 → j') scattering that the integral cross sections on our potential indeed show the predicted[53] propensity for even Δj transitions and are in close agreement with the cross sections calculated on the 2D CCSD(T) and MRCI potentials of Shepler et al.[23] Since the latter potentials were also calculated with special attention for the accuracy in the long range, this confirms that also our potential is accurate in that region.

4.2. Vibrational Frequencies and Rotational Constants of HCO. A series of vibrational frequencies of HCO was obtained from laser photoelectron spectroscopy of the formyl anion by Murray et al.[14] and with the use of dispersed fluorescense and stimulated emission pumping spectroscopy of HCO by Tobiason et al.[8] The ground-state rotational and distortion constants were measured by microwave spectroscopy[50] and, later, by magnetic resonance far-infrared laser spectroscopy.[54,55] The best way to check our 3D H−CO potential is to use it in accurate calculations of the rovibrational states of HCO and directly compare the results with these experimental data. Actually, the modified BBH potential[6,7] is a scaled version of the ab initio BBH potential,[5] modified such that the vibrational frequencies agree better with the experimental data of.[14,16] Similarly, the modified WKS potential[10] was obtained from the ab initio WKS potential[9] by scaling to improve agreement with the more recent vibrational frequencies of ref 8. The method that we used to compute the vibrational states of HCO is the 3D DVR method in Jacobi coordinates with the program of Tennyson et al.[56] The radial Gauss−Laguerre quadrature grids contained 20 points in the r coordinate and 25 points in R. For the angle θ we used 45 point Gauss−Legendre quadrature. In tests with smaller and larger numbers of DVR grid points, we confirmed that the vibrational levels are converged to about 0.001 cm^{-1} for the lower levels and to about 0.005 cm^{-1} for the levels at 5000 cm^{-1} above the zero-point level.

An important result from these calculations is the vibrational zero-point energy of HCO. We mentioned above that the binding energy D_e relative to the free H atom and the free CO molecule at its equilibrium geometry is 30.6973 mE_h = 0.8353 eV. The lowest level obtained from the 3D DVR calculations lies 2794.95 cm^{-1} = 0.3465 eV above the global minimum in the potential, in other words the vibrational zero-point energy of HCO is 0.3465 eV. Since we also calculated the zero-point vibrational energy of free CO, 0.1341 eV, we obtain the dissociation energy D_0 of H−CO: 0.623 eV. Two values of the H−CO bond enthalpy at 298 K have been measured by Chuang et al.[15] and by Walsch, quoted in ref 9. If these enthalpies are converted[9] to 0 K bond energies, the D_0 values are 0.629 ± 0.008 eV and 0.603 ± 0.009 eV, respectively. Our ab initio value agrees well with these data. The WKS potential gave D_0 = 0.569 eV[9] and the empirically modified WKS potential gave D_0 = 0.620 eV.[10]

The vibrational frequencies from the 3D DVR calculations for total angular momentum J = 0 are listed and compared with the most recent experimental data[8] in Table 5. The agreement with the measured frequencies is good, nearly as good as for the modified WKS potential and better than for the modified BBH potential—both these potentials were scaled to get agreement

dx.doi.org/10.1021/jp402470b | J. Phys. Chem. A 2013, 117, 7571−7579

Table 5. Calculated and Experimental Vibrational Term Energies (in cm^{-1}) of the Bound Levels of $\tilde{X}^2A'$ HCO (J = 0)[a]

assignment	experimental	calculated	deviation
(0,0,1)	1080.76	1079.6	−0.11%
(0,1,0)	1868.17	1871.6	0.18%
(0,0,2)	2142	2145.2	0.15%
(1,0,0)	2434.48	2428.5	−0.25%
(0,1,1)	2942	2950.0	0.27%
(0,0,3)	3171	3186.2	0.48%
(1,0,1)	3476	3464.1	−0.34%
(0,2,0)	3709	3719.0	0.27%
(0,1,2)	3997	4013.1	0.40%
(0,0,4)	4209*	4195.7	−0.32%
(1,1,0)	4302	4301.5	−0.01%
(1,0,2)	4501*	4478.7	−0.50%
(2,0,0)	4570*	4546.0	−0.53%
(0,2,1)	4783.2	4797.2	0.29%

[a]Most of the experimental data are from Tobiason et al.,[8] the data marked with * are from Rumbles et al.[17] The assignment (v_1,v_2,v_3) is in terms of the CH stretch level v_1, the CO stretch level v_2, and the ∠HCO bend quantum number v_3.

with the experimental vibrational frequencies—and substantially better than with the original ab initio WKS and BBH potentials. Furthermore, we computed the levels for higher rotational states of HCO, up to J = 6. Then, we extracted the rotational constants A, B, C and the centrifugal distortion constants Δ_J, Δ_{JK}, Δ_K of HCO in its vibrational ground state from a fit of the rotational levels to the eigenvalues of the usual semirigid rotor Hamiltonian for a prolate near-symmetric top including centrifugal distortion

$$\hat{H}_{\mathrm{rot}} = \frac{1}{2}(B + C)\hat{\mathbf{J}}^2 + \left[A - \frac{1}{2}(B + C)\right]\hat{J}_z^2 + \frac{1}{4}(B - C)(\hat{J}_+^2 + \hat{J}_-^2) + \Delta_J\hat{\mathbf{J}}^4 + \Delta_{JK}\hat{\mathbf{J}}^2\hat{J}_z^2 + \Delta_K\hat{J}_z^4 \quad (9)$$

where $\hat{\mathbf{J}}$ is the total angular momentum operator, $\hat{J}_z$ its projection on the long (a) axis, and $\hat{J}_\pm$ are step-up and step-down operators. The approximate quantum number K is the eigenvalue of $\hat{J}_z$. We did not include off-diagonal centrifugal distortion terms, because their effect on the energy levels is smaller than the remaining convergence error of the rotational levels calculated. It turned out that Δ_J and Δ_{JK} are also very small (as they are experimentally[54]) and not well converged; the distortion constant Δ_K is significant, however.

Table 6 gives the results and their comparison with the experimental data.[54,55] Small variations occur in the values of A, B, and C fit to our rotational levels, depending on the highest J value for which these levels were included in the fit. Also spin−orbit coupling constants were fitted to the measured spectra[54,55] of ground state HCO($\tilde{X}^2A'$), but we did not include spin−orbit coupling in our calculations of the rovibrational levels, so we cannot compare these parameters. The rotational constants A, B, C and the relatively large centrifugal distortion constant Δ_K extracted from the rotational levels agree very well with the experimental data. It is easily checked, for example, that the small discrepancy of 0.5% in the value of A corresponds to a change of ∠HCO of only 0.1°. Also the rotational constants calculated with the assumption that HCO is fixed at its equilibrium geometry, with R_{CH} = 2.115 a_0, r = 2.221 a_0, and ∠HCO = 124.6°, are included in Table 6. The deviations between these equilibrium geometry values and the values from the full 3D calculations are larger than the differences between the latter and the experimental values. This illustrates that the direct comparison of the rotational constants calculated for the vibrational ground state with the corresponding experimental data is to be preferred over the comparison of geometric parameters extracted from spectroscopic data, as shown in Table 2. The agreement with the experimental vibrational frequencies and rotational constants, obtained directly with our 3D ab initio potential surface without any adaptation, demonstrates that this potential is indeed accurate.

Table 6. Calculated and Experimental[54,55] Rotational and Distortion Constants (in cm^{-1}) of $\tilde{X}^2A'$ HCO in Its Vibrational Ground (v_1,v_2,v_3) = (0,0,0) State

J_{max}	K_{max}	A	B	C	$10^3\Delta_K$	fit error
4	4	24.4804	1.4945	1.4030	29.4453	0.012
5	5	24.4640	1.4955	1.4045	27.9362	0.041
6	6	24.4392	1.4971	1.4066	26.3809	0.100
experiment		24.3296	1.4940	1.3987	31.4042(57)	
equilibrium structure		24.2667	1.4968	1.4099		

5. CONCLUSIONS

We constructed an accurate analytical 3D potential energy surface for the H−CO($\tilde{X}^2A'$) complex based on high-level RHF-UCCSD(T)/CBS ab initio calculations. Both by extending the calculated data points to large values of the H−CO distance R and by taking special care in the fit procedure, we ensured that this potential is also accurate in the long-range region. This will be important for the application of the potential in calculating H−CO inelastic collision cross sections, especially at lower energies. Integral cross sections for rotationally inelastic H−CO(j = 0 → j') collisions were obtained with the close-coupling method. The CO molecule was considered as a rigid rotor, in order to be able to compare the results with cross sections calculated on two different 2D potentials for H−CO. The agreement is very good, which confirms that our potential is accurate in the long-range. Furthermore, we applied our potential in calculations of the rovibrational states of HCO with the use of a 3D DVR method. The ab initio dissociation energy D_0 = 0.623 eV obtained from this calculation agrees well with experimental data. Also, the vibrational levels resulting from the DVR calculations are in good agreement with experimental data, better than those from previous ab initio potentials and nearly as good as those from the semiempirical "modified WKS potential" that was scaled for better agreement with these vibrational levels. From the rotational levels of HCO in its vibrational ground state for total angular momentum J = 0−6 we extracted the rotational constants A, B, C, and the dominant centrifugal distortion constant Δ_K. Also, they agree well with measured data. This confirms that our potential is also accurate in the region of the potential well.

Further studies are planned to investigate vibration−rotation inelastic collision processes. Integral and differential cross sections will be obtained from full 3D close-coupling calculations. The differential cross sections will be compared with results from crossed beam experiments combined with velocity map imaging that will soon be performed. The integral

dx.doi.org/10.1021/jp402470b | J. Phys. Chem. A 2013, 117, 7571−7579

cross sections and rate constants will be used in modeling astrophysical processes.

■ ASSOCIATED CONTENT

Supporting Information

The Supporting Information contains: Example input file to compute the H−CO interaction energy with the MOLPRO package; a list of all ab initio calculated interaction energies and the corresponding coordinates; a Fortran program to evaluate our 3D potential surface of HCO, with a test program that calls it and compares it with the corresponding ab initio values. This material is available free of charge via the Internet at http://pubs.acs.org.

■ AUTHOR INFORMATION

Corresponding Author

*E-mail: gerritg@theochem.ru.nl.

Notes

The authors declare no competing financial interest.

■ ACKNOWLEDGMENTS

We acknowledge funding by The Netherlands Organisation for Scientific Research, NWO, through the Dutch Astrochemistry Network. We thank Prof. Jonathan Tennyson for making available the program DVR3D applied in our bound state calculations and Prof. W. Leo Meerts for the fit program used to extract the rotational constants of HCO from our calculated rotational energy levels. Prof. Naduvalath Balakrishnan is thanked for sending the potentials and results of ref.[23] and Prof. Stefan Andersson for sending his unpublished 3D HCO potential.

■ REFERENCES

(1) Schöier, F. L.; van der Tak, F. F. S.; van Dishoeck, E. F.; Black, J. H. An atomic and molecular database for analysis of submillimetre line observations. *Astron. Astrophys.* **2005**, *432*, 369.

(2) van der Tak, F. F. S.; Black, J. H.; Schöier, F. L.; Jansen, D. J.; van Dishoeck, E. F. A computer program for fast non-LTE analysis of interstellar line spectra. *Astron. Astrophys.* **2007**, *468*, 627.

(3) González-Alfonso, E.; Wright, C. M.; Cernicharo, J.; Rosenthal, D.; Boonman, A. M. S.; van Dishoeck, E. F. CO and H_2O vibrational emission toward Orion Peak 1 and Peak 2. *Astron. Astrophys.* **2002**, *386*, 1074.

(4) Liszt, H. S. Rotational excitation of CO in a cool, mixed atomic and molecular hydrogen gas. *Astron. Astrophys.* **2006**, *458*, 507.

(5) Bowman, J. M.; Bittman, J. S.; Harding, L. B. *Ab initio* calculations of electronic and vibrational energies of HCO and HOC. *J. Chem. Phys.* **1986**, *85*, 911.

(6) Bowman, J. M.; Gazdy, B. A simple method to adjust potential energy surfaces: Application to HCO. *J . Chem. Phys.* **1991**, *94*, 816.

(7) Wang, D.; Bowman, J. M. Complex L^2 calculations of bound states and resonances of HCO and DCO. *Chem. Phys. Lett.* **1995**, *235*, 277.

(8) Tobiason, J. D.; Dunlop, J. R.; Rohlfing, E. A. The unimolecular dissociation of HCO: A spectroscopic study of resonance energies and widths. *J. Chem. Phys.* **1995**, *103*, 1448.

(9) Werner, H.-J.; Bauer, C.; Rosmus, P.; Keller, H.-M.; Stumpf, M.; Schinke, R. The unimolecular dissociation of HCO: I. Oscillations of pure CO stretching resonance widths. *J. Chem. Phys.* **1995**, *102*, 3593.

(10) Keller, H.-M.; Floethmann, H.; Dobbyn, A. J.; Schinke, R.; Werner, H.-J.; Bauer, C.; Rosmus, P. The unimolecular dissociation of HCO. II. Comparison of calculated resonance energies and widths with high-resolution spectroscopic data. *J. Chem. Phys.* **1996**, *105*, 4983.

(11) Gray, S. K. Wave packet dynamics of resonance decay: An iterative equation approach with application to HCO → H+CO. *J. Chem. Phys.* **1992**, *96*, 6543.

(12) Dixon, R. N. A three-dimensional time-dependent wavepacket calculation for bound and quasi-bound levels of the ground state of HCO: Resonance energies, level widths and CO product state distributions. *J. Chem. Soc., Faraday Trans.* **1992**, *88*, 2575.

(13) Wang, D.; Bowman, J. M. L^2 calculations of resonances and final rotational distributions for HCO → H+CO. *J. Chem. Phys.* **1994**, *100*, 1021.

(14) Murray, K. K.; Miller, T. M.; Leopold, D. G.; Lineberger, W. C. Laser photoelectron spectroscopy of the formyl anion. *J. Chem. Phys.* **1986**, *84*, 2520.

(15) Chuang, M.-C.; Foltz, M. F.; Moore, C. B. T_1 barrier height, S_1−T_1 intersystem crossing rate, and S_0 radical dissociation threshold for H_2CO, D_2CO, and HDCO. *J. Chem. Phys.* **1987**, *87*, 3855.

(16) Sappey, A. D.; Crosley, D. R. Laser-induced fluorescence in the $\tilde{B}$−$\tilde{X}$ system of the HCO radical. *J. Chem. Phys.* **1990**, *93*, 7601.

(17) Rumbles, G.; Lee, E. K. C.; Valentini, J. J. Laser-induced fluorescence from the predissociating formyl radical. Part 2. Analysis of dispersed emission from the $\tilde{A}$−X transition. *J. Chem. Soc., Faraday Trans.* **1990**, *86*, 3837.

(18) Adamson, G. W.; Zhao, X. S.; Field, R. W. The HCO $\tilde{B}^2A' \leftrightarrow \tilde{X}^2A'$ system: Fluorescence excitation and stimulated emission pumping spectra. *J. Mol. Spectrosc.* **1993**, *160*, 11.

(19) Neyer, D. W.; Luo, X.; Burak, I.; Houston, P. L. Photodissociation dynamics of state-selected resonances of HCO $\tilde{X}^2A'$ prepared by stimulated emission pumping. *J. Chem. Phys.* **1995**, *102*, 1645.

(20) McBane, G. C.; Kable, S. H.; Houston, P. L.; Schatz, G. C. Collisional excitation of CO by 2.3 eV H atoms. *J. Chem. Phys.* **1991**, *94*, 1141.

(21) Green, S.; Pan, B.; Bowman, J. M. Quantum scattering calculations for vibrational and rotational excitation of CO by hot hydrogen atoms. *J. Chem. Phys.* **1995**, *102*, 8800.

(22) Green, S.; Keller, H.-M.; Schinke, R.; Werner, H.-J. Vibration−rotation excitation of CO by hot hydrogen atoms: Comparison of two potential energy surfaces. *J. Chem. Phys.* **1996**, *105*, 5416.

(23) Shepler, B. C.; Yang, B. H.; Dhilip Kumar, T. J.; Stancil, P. C.; Bowman, J. M.; Balakrishnan, N.; Zhang, P.; Bodo, E.; Dalgarno, A. Low energy H+CO scattering revisited. *Astron. Astrophys.* **2007**, *475*, L15.

(24) Werner, H.-J.; Knowles, P. J. A second order multiconfiguration SCF procedure with optimum convergence. *J. Chem. Phys.* **1985**, *82*, 5053.

(25) Knowles, P. J.; Werner, H.-J. An efficient second-order MC SCF method for long configuration expansions. *Chem. Phys. Lett.* **1985**, *115*, 259.

(26) Dunning, T. H. Gaussian basis sets for use in correlated molecular calculations. I. The atoms boron through neon and hydrogen. *J. Chem. Phys.* **1989**, *90*, 1007.

(27) Helgaker, T.; Jørgensen, P.; Olsen, J. *Molecular Electronic Structure Theory*; Wiley: Chichester, U.K., 2000.

(28) Knowles, P. J.; Hampel, C.; Werner, H.-J. Coupled cluster theory for high spin, open shell reference wave functions. *J. Chem. Phys.* **1993**, *99*, 5219.

(29) Knowles, P. J.; Hampel, C.; Werner, H.-J. Erratum: "Coupled cluster theory for high spin, open shell reference wave functions" [J. Chem. Phys. 99, 5219 (1993)]. *J. Chem. Phys.* **2000**, *112*, 3106.

(30) Watts, J. D.; Gauss, J.; Bartlett, R. J. Coupled-cluster methods with noniterative triple excitations for restricted open-shell Hartree−Fock and other general single determinant reference functions. Energies and analytical gradients. *J. Chem. Phys.* **1993**, *98*, 8718.

(31) Werner, H.-J.; Knowles, P. J.; et al., MOLPRO: A package of *ab initio* programs, version 2010.1. http://www.molpro.net.

(32) van Mourik, T.; Dunning, T. H. A new *ab initio* potential energy curve for the helium dimer. *J. Chem. Phys.* **1999**, *111*, 9248.

(33) van Mourik, T.; Wilson, A. K.; Dunning, T. H. Benchmark calculations with correlated molecular wavefunctions. XIII. Potential

energy curves for He_2, Ne_2, and Ar_2 using correlation consistent basis sets through augmented sextuple zeta. *Mol. Phys.* **1999**, *96*, 529.
(34) Boys, S. F.; Bernardi, F. The calculation of small molecular interactions by the differences of separate total energies. Some procedures with reduced errors. *Mol. Phys.* **1970**, *19*, 553.
(35) Lee, T. J.; Taylor, P. R. A diagnostic for determining the quality of single-reference electron correlation methods. *Int. J. Quantum. Chem. Symp.* **1989**, *23*, 199.
(36) Jayatilaka, D.; Lee, T. J. Open-shell coupled-cluster theory. *J. Chem. Phys.* **1993**, *98*, 9734.
(37) Lee, T. J. Comparison of the T_1 and D_1 diagnostics for electronic structure theory: A new definition for the open-shell D_1 diagnostic. *Chem. Phys. Lett.* **2003**, *372*, 362.
(38) Le Floch, A. Revised molecular constants for the ground state of CO. *Mol. Phys.* **1991**, *72*, 133.
(39) Le Roy, R. J. *RKR1 2.0: A computer program implementing the first-order RKR method for determining diatomic molecule potential energy curves*; University of Waterloo Chemical Physics Research Report No. CP-657, 2004 (http://leroy.uwaterloo.ca/programs/).
(40) Tikhonov, A. N.; Arsenin, V. Y. *Solutions of Ill-Posed Problems*; Wiley: New York, 1977.
(41) van der Avoird, A.; Wormer, P. E. S.; Mulder, F.; Berns, R. M. *Ab initio* studies of the interactions in Van der Waals molecules. *Top. Curr. Chem.* **1980**, *93*, 1.
(42) Tang, K. T.; Toennies, J. P. An improved simple model for the van der Waals potential based on universal damping functions for the dispersion coefficients. *J. Chem. Phys.* **1984**, *80*, 3726.
(43) Ho, T.-S.; Rabitz, H. A general method for constructing multidimensional molecular potential energy surfaces from *ab initio* calculations. *J. Chem. Phys.* **1996**, *104*, 2584.
(44) Ho, T.-S.; Rabitz, H. Proper construction of *ab initio* global potential surfaces with accurate long-range interactions. *J. Chem. Phys.* **2000**, *113*, 3960.
(45) Colbert, D. T.; Miller, W. H. A novel discrete variable representation for quantum mechanical reactive scattering via the S-matrix Kohn method. *J. Chem. Phys.* **1992**, *96*, 1982.
(46) Groenenboom, G. C.; Colbert, D. T. Combining the discrete variable representation with the S-matrix Kohn method for quantum reactive scattering. *J. Chem. Phys.* **1993**, *99*, 9681.
(47) Krupenie, P. H.; Weissman, S. Potential-Energy Curves for CO and CO^+. *J. Chem. Phys.* **1965**, *43*, 1529.
(48) Yardley, J. T. Laser action in highly-excited vibrational levels of CO. *J. Mol. Spectrosc.* **1970**, *35*, 314.
(49) Mantz, A. W.; Maillard, J.-P.; Roh, W. B.; Rao, K. N. Ground state molecular constants of $^{12}C^{16}O$. *J. Mol. Spectrosc.* **1975**, *57*, 155.
(50) Austin, J. A.; Levy, D. H.; Gottlieb, C. A.; Radford, H. E. Microwave spectrum of the HCO radical. *J. Chem. Phys.* **1974**, *60*, 207.
(51) Johns, J. W. C.; Priddle, S. H.; Ramsay, D. A. Electronic absorption spectra of HCO and DCO radicals. *Discuss. Faraday Soc.* **1963**, *35*, 90.
(52) Wang, H. Y.; Eyre, J. A.; Dorfman, L. M. Activation energy for the gas phase reaction of hydrogen atoms with carbon monoxyde. *J. Chem. Phys.* **1973**, *59*, 5199.
(53) Lee, K.-T.; Bowman, J. M. Rotational distributions from resonant and direct scattering in H+CO and tests of statistical theories. *J. Chem. Phys.* **1987**, *86*, 215.
(54) Sears, T. J. The calculation of the energy levels of an asymmetric top free radical in a magnetic field. *Comput. Phys. Rep.* **1984**, *2*, 1.
(55) Brown, J. M.; Radford, H. E.; Sears, T. J. Avoided crossings in the far-infrared laser magnetic resonance spectrum of HCO. *J. Mol. Spectrosc.* **1991**, *148*, 20.
(56) Tennyson, J.; Kostin, M. A.; Barletta, P.; Harris, G. J.; Polyansky, O. L.; Ramanlal, J.; Zobov, N. F. DVR3D: A program suite for the calculation of rotation-vibration spectra of triatomic molecules. *Comput. Phys. Commun.* **2004**, *163*, 85.